Title	Giant mesoscopic spin hall effect on the surface of topological insulator
Author(s)	Gao, JH; Yuan, J; Chen, WQ; Zhou, Y; Zhang, FC
Citation	Physical Review Letters, 2011, v. 106 n. 5
Issued Date	2011
URL	http://hdl.handle.net/10722/139611
Rights	Physical Review Letters. Copyright © American Physical Society.

Giant Mesoscopic Spin Hall Effect on the Surface of Topological Insulator

Jin-Hua Gao,[1] Jie Yuan,[1] Wei-Qiang Chen,[1] Yi Zhou,[2] and Fu-Chun Zhang[1,2]

[1]*Department of Physics, and Center of Theoretical and Computational Physics, The University of Hong Kong, Hong Kong, China*

[2]*Department of Physics, Zhejiang University, Hangzhou, China*

(Received 5 October 2010; published 2 February 2011)

We study mesoscopic spin Hall effect on the surface of a topological insulator with a step-function potential by using the McMillan method commonly used in the study of superconductor junctions. In the ballistic transport regime, we predict a giant spin polarization induced by a transverse electric current with parameter suitable to the topological insulator thin film Bi_2Se_3. The spin polarization oscillates across the potential boundary with no confinement due to the Klein paradox, and should be observable in a spin resolved scanning tunneling microscope.

DOI: 10.1103/PhysRevLett.106.057205 PACS numbers: 85.75.−d, 72.25.−b, 73.20.−r, 73.23.−b

The field of a topological insulator (TI) with time reversal invariance has been exploring recently [1–9]. In a three-dimensional (3D) TI, the electronic structure is characterized by a bulk gap and a gapless surface mode of Dirac particles. The topological properties are protected by time reversal symmetry. The surface states in the TI are helical, where electron spins are locked to their momenta. Both the Dirac dispersion of the surface states and the spin-momentum correlation have been confirmed in experiments [6,7]. Because of the strong correlation between the spin and momentum, these surface states are natural candidates for studying spintronics, where the electron's spin degree is used to manipulate and to control mesoscopic electronic devices.

The spin Hall effect (SHE) refers to a boundary (surface or edge) spin polarization when an electric current is flowing through the system. It is interesting to note that recent advances in the SHE and the quantum SHE have greatly contributed to the development of the field of the TI. There have been extensive studies on the SHE in the conventional semiconductors or metals with spin-orbit coupling [10–19]. The SHE is often classified into ''extrinsic'' (impurity driven) or ''intrinsic'' (band structure driven). Since arbitrarily weak disorder destroys the intrinsic SHE in a 2D infinite system with linear spin-orbit coupling [20,21], current interest is focusing on the mesoscopic systems in the ballistic regime, where the disorder may be ignored [22–27]. In the ballistic regime, the electric field is absent inside the system, and the spin polarization is resulted from the spin precession around the lateral confined potential. In 2D semiconductor systems, ballistic spin polarization has been predicted near the potential barrier [23,24,26]. However, the effect has not been observed in experiments because of the weakness of the effect in realistic semiconductors, and because of the difficulty in detecting the spatial distribution of the spin polarization in the sandwiched interface. The surface state of the TI represents a different type of 2D system, where the spin-orbit coupling is strong and the surface state can be probed directly by a scanning tunneling microscope (STM). As pointed out by Silvestrov and Mischenko [28], one expects an enhancement of spin polarization in the TI for there is no quadratic dependence of the spin-orbit coupling strength as in semiconductor heterostructures. This may provide a new route in the study of the SHE [28,29] and spintronics in general.

In this Letter, we report the theoretical prediction of a giant mesoscopic SHE (MSHE, current-induced spin polarization) on a surface of 3D TI thin film with a step-function potential in the ballistic regime as schematically illustrated in Fig. 1. By using the McMillan-Green function method, which is commonly used in study of superconductor junctions, we derive analytic expressions for the electric current-induced spin polarization. The spin polarization is found to oscillate across the potential boundary, and is not confined by the potential due to the Klein paradox. For the parameters suitable to TI thin film Bi_2Se_3, the amplitude of the local spin polarization is estimated to be as large as 20% at the Fermi level near the boundary, which is much larger than that in typical 2D systems, and should be observable in spin resolved STM.

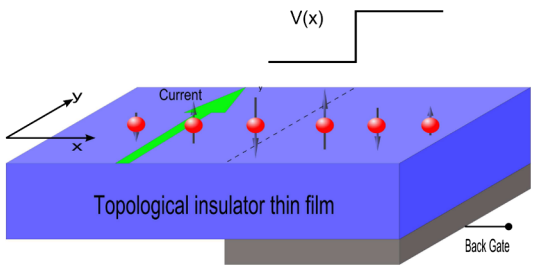

FIG. 1 (color online). Schematic illustration of the proposed mesoscopic spin Hall effect on the surface (x-y plane) of a topological insulator. A back gate of voltage V_2 is applied at the right side with $x > 0$. Electric current flows along the y direction, resulting in spin polarization oscillation along the x direction across the barrier.

We consider surface states of TI, described by an effective Hamiltonian in the x-y plane,

$$H = v_F(\boldsymbol{p} \times \boldsymbol{\sigma}) \cdot \hat{z} + V(x), \tag{1}$$

where $\boldsymbol{p}$ is the electron momentum, $\boldsymbol{\sigma}$ are the Pauli matrices, and v_F is the Fermi velocity. The system is translational invariant along the y axis, and has a step-function potential at $x = 0$, which separates two regions along the x axis: region 1 at $x < 0$ and region 2 at $x > 0$, as illustrated in Fig. 1,

$$V(x) = \begin{cases} V_1 = 0 & \text{if } x < 0; \\ V_2 & \text{if } x > 0 \end{cases}$$

where V_2 is a constant. A voltage of V_y is applied across the surface to induce an electric current along the y direction. The step-function potential can be realized by applying a back gate. The back gating in the TI thin film samples with a thickness of 10 and 50 nm has been reported in a recent experiment [30]. The thin film of TI possesses the same gapless Dirac modes, provided that the thin film is thicker than a critical thickness of about 6 nm or 6 quintuple layers, as demonstrated in recent experiment [31]. This allows us to have proper TI samples whose physics is described by Eq. (1).

We consider the ballistic regime, where the electric field inside the surface is zero. We will first construct the retarded Green's function with the scattering wave functions, a method introduced by McMillan [32]. We then calculate the local spin density in the presence of an electric current to show the profound MSHE, discuss experimental consequences, and compare the MSHE in TI with that in a conventional 2D electron system with Rashba coupling.

The scattering wave functions can be constructed based on the eigenfunctions of the Dirac particle in Hamiltonian (1) in the two separate spatial regions. The eigen wave functions in region α corresponding to the energy ϵ and y-component momentum k_y are given by

$$\varphi_\alpha^{\pm}(x, y) = e^{i(\pm k_{\alpha x} \cdot x + k_y \cdot y)} \begin{pmatrix} 1 \\ i\hbar v_F \frac{\pm k_{\alpha x} + i k_y}{\epsilon - V_\alpha} \end{pmatrix} \tag{2}$$

where $\hbar v_F k_{\alpha x} = \sqrt{(\epsilon - V_\alpha)^2 - (\hbar v_F k_y)^2}$. By adjusting the gate potential V_α relative to the Fermi energy E_F, the Dirac fermion carriers in region α can be tuned into electronlike (n type, $E_F > V_\alpha$) or holelike (p type, $E_F < V_\alpha$). Therefore, the system may be viewed as n-n or n-p types of junctions.

The right (R) and left (L) moving scattering wave functions can then be found by using the standard transfer matrix method. For a n-n junction, we have

$$\phi_R^{nn}(x, y) = \begin{cases} \varphi_1^+(x, y) + r_R^{nn} \varphi_1^-(x, y) & \text{if } x < 0 \\ t_R^{nn} \varphi_2^+(x, y) & \text{if } x > 0 \end{cases}$$

$$\phi_L^{nn}(x, y) = \begin{cases} t_L^{nn} \varphi_1^-(x, y) & \text{if } x < 0 \\ \varphi_2^-(x, y) + r_L^{nn} \varphi_2^+(x, y) & \text{if } x > 0 \end{cases} \tag{3}$$

where $t_{R/L}^{nn}$ and $r_{R/L}^{nn}$ are the transmission and reflection coefficients, respectively, which are related by

$$\begin{pmatrix} t_R^{nn} \\ 0 \end{pmatrix} = T \begin{pmatrix} 1 \\ r_R^{nn} \end{pmatrix}, \qquad \begin{pmatrix} r_L^{nn} \\ 1 \end{pmatrix} = T \begin{pmatrix} 0 \\ t_L^{nn} \end{pmatrix}$$

where T is the transfer matrix, whose explicit form can be found in the supplementary material [33]. The scattering wave functions for a n-p junction have a similar form, except that all the superindices of nn are replaced by np and that $\varphi_2^{+(-)}$ are replaced by $\varphi_2^{-(+)}$ in the region $x > 0$ because the group velocity of a hole is opposite to that of an electron.

If k_x is complex, the evanescent wave appears. In this case, considering the asymptotic behavior of the evanescent wave, the scattering wave function for both n-n and n-p junction will have the form given in Eq. (3).

We are interested in the transverse effect of the charge and spin density profiles as an electric voltage is applied along the y axis. To this end, we use the McMillan method [32] to construct the retarded Green's function from the scattering wave functions. The retarded Green's function satisfies the equation,

$$(\epsilon - H) G^r(x, x'; \epsilon, k_y) = \delta(x - x') I \tag{4}$$

where I is a 2 by 2 identity matrix. The solution for G^r is a direct product of the scattering wave functions $\phi_{R/L}$ and the transposal wave functions $\hat{\phi}_{L/R}^t$ [32],

$$G^r(x, x'; \epsilon, k_y) = \begin{cases} c^< \phi_L(x, y) \hat{\phi}_R^t(x', y) & \text{if } x < x' \\ c^> \phi_R(x, y) \hat{\phi}_L^t(x', y) & \text{if } x > x' \end{cases} \tag{5}$$

where $c^<$ and $c^>$ are the coefficients, which can be determined from Eq. (4). Here, $\hat{\phi}_{L/R}$ has the same form as $\phi_{L/R}$ except the replacement of the factor $e^{ik_y \cdot y}$ by $e^{-ik_y \cdot y}$.

The local spin density of states $\mathbf{S}$ for a given k_y and the local charge density of states ρ at energy ϵ can be found easily from G^r,

$$\boldsymbol{S}(x; \epsilon, k_y) = -\frac{\hbar}{2\pi} \operatorname{Im} \operatorname{Tr}[G^r(x, x; \epsilon, k_y) \boldsymbol{\sigma}], \tag{6}$$

$$\rho(x, \epsilon) = -\frac{1}{\pi} \sum_{k_y} \operatorname{Im} \operatorname{Tr} G^r(x, x; \epsilon, k_y), \tag{7}$$

where the sum in ρ is over all the possible values of k_y, and the contributions from the evanescent waves are also included. In the present case, the Green's function, the local charge and spin density of states, can be solved analytically. Here we shall focus on the spin z component, and the charge density of states [33].

The local spin density of states for a given k_y in the n-n and n-p junctions are plotted in Fig. 2. One important feature is the nonconfinement of the Dirac particle with the higher barrier potential ($V_2 > \epsilon$) due to the Klein paradox. The local spin density strongly depends on the incident angle of the electron, as we can see from Fig. 2. The evanescent wave appears if $|\epsilon - V_1| > \hbar v_F k_y > |\epsilon - V_2|$,

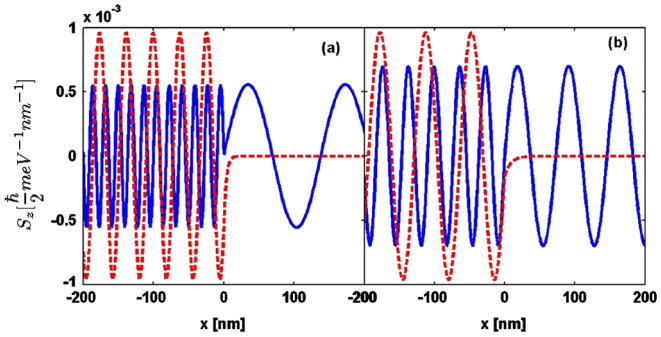

FIG. 2 (color online). Spatial distribution of local spin density S_z for a single Dirac fermion in Hamiltonian (1) with $v_F = 5 \times 10^5$ m/s, the Fermi velocity of the surface state of TI Bi_2Se_3 as measured in experiment [7] and also predicted in band calculations [9]. (a) n-n junction, $V_2 = 40$ meV, and $\epsilon = 60$ meV. $\theta = 63°$ [(blue) solid line] and $\theta = 18°$ [(red) dashed line]. (b) n-p junction, $V_2 = 60$ meV, and $\epsilon = 35$ meV. $\theta = 63°$ [(blue) solid line] and $\theta = 36°$ [(red) dashed line]. θ is an incident angle, defined by $e^{i\theta} = \frac{k_x + ik_y}{|\epsilon - V|}$.

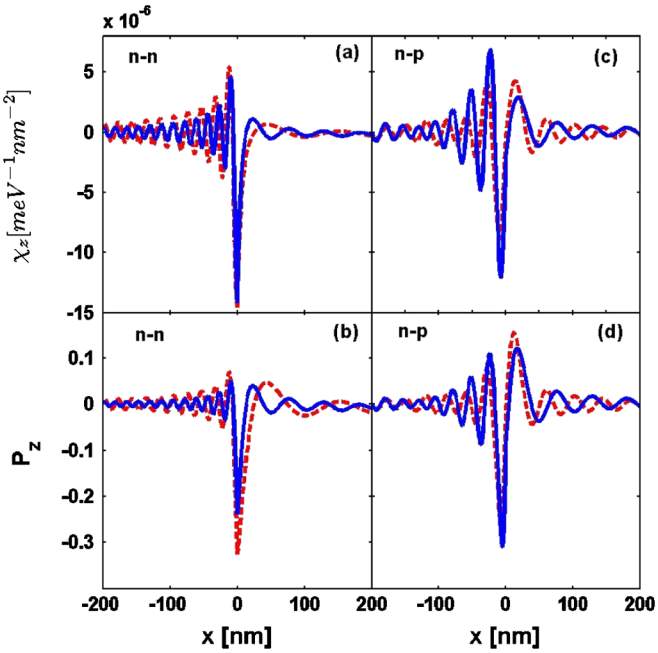

FIG. 3 (color online). Spatial profiles of spin polarization density $\chi_z(x; E_F)$ (top panels), and spin polarization $P_z(x; E_F)$ (bottom panels) on the surface of TI, described by Eq. (1) with $v_F = 5 \times 10^5$ m/s, suitable for Bi_2Se_3. Left panels (a) and (b) are for n-n junction: $V_1 = 0$, $V_2 = 40$ meV, and the Fermi energy $E_F = 50$ meV [(red) dashed line] and $E_F = 60$ meV [(blue) solid line]. Right panels (c) and (d) are for n-p junction: $V_1 = 0$, $V_2 = 60$ meV, and $E_F = 35$ meV [(red) dashed lines] and $E_F = 40$ meV [(blue) solid lines]. $P_z = 1$ corresponds to completely polarized spins at E_F.

and there is a critical incident angle for the condition of the evanescent wave. These features are typical characteristics of a Dirac fermion, essentially the same as in the graphene [34].

We now calculate the spin polarization along x direction near the potential boundary $x = 0$, induced by an electric current along the y direction at zero temperature. We consider a voltage of $V_y/2$ at the one edge and $-V_y/2$ at the other edge of the system along the y axis, and consider the ballistic transport limit. The effect of the voltage at the two edges is to induce an imbalance of the occupied states between $k_y > 0$ and $k_y < 0$. The states with $k_y > 0$ are occupied at energies below $E_F + V_y/2$, and the states with $k_y < 0$ are occupied at energies below $E_F - V_y/2$, with E_F the Fermi energy at $V_y = 0$. By the time reversal symmetry, the local spin polarizations contributed from $k_y > 0$ and from $k_y < 0$ with the same energy cancel to each other. For small value of V_y, we thus obtain the current-induced net spin density profile [23,24,35]

$$S_z^{\text{in}}(x; E_F) \simeq |eV_y| \sum_{k_y > 0} S_z(x; E_F, k_y) \tag{8}$$

To further analyze the current-induced spin polarization, we define local spin susceptibility $\chi_z(x; E_F)$ and local spin polarization $P_z(x; E_F)$,

$$\begin{aligned} \chi_z(x; E_F) &= S_z^{\text{in}}(x; E_F) / \frac{\hbar}{2} eV_y \\ P_z(x; E_F) &= \chi_z(x; E_F) / \rho(x; E_F). \end{aligned} \tag{9}$$

The local spin polarization P_z is a dimensionless parameter to measure the magnitude of the MSHE. $P_z = 1$ means the spins of the electrons at a space point x at the Fermi level are polarized. The experimentally measured local spin density is obtained via multiplying P_z by the applied voltage and by the local density of states. In Fig. 3, we plot χ_z and the P_z for both n-n and n-p junctions. The key features of the MSHE in the system are summarized below. (i) There is a pronounced oscillation of spin polarization near the potential boundary $x = 0$. The peak value of χ_z is of the order of 10^{-6} meV^{-1} nm^{-2}, and the peak value of P_z is about 20%, indicating the MSHE here is giant. (ii) The induced spin polarization is found to be insensitive to the Fermi energy on the TI surface. This may be understood because the spin polarization is approximately inversely proportional to v_F, and v_F is a constant for Dirac particles. This is markedly different from the usual 2D system where v_F is proportional to $\sqrt{E_F}$; hence, the spin polarization is a function of E_F. The oscillation period at the zero gate region is inversely proportional to the Fermi wave vector, or $1/k_F = \hbar v_F / E_F$, typically tens of nanmoeters for E_F at tens of milli-electron volts. The period at the bottom gated region is proportional to $\hbar v_F / |E_F - V_2|$, and can be larger. The spin polarization predicted in our theory may be detected in spin resolved STM TI samples with a mean free path over several micron. Different from the 2D electron gas in semiconductors, formed in a sandwiched interface which is difficult to carry out in STM, the surface of TI can be directly measured by STM. The bottom gated

device allows us to detect the spin polarizations at both left and right regions.

The predicted MSHE on the TI surface is much larger than those in the ballistic 2D electron system with Rashba spin-orbit coupling. The latter effect is relatively weak and has not been observed in experiment. In the 2D electron system, $v_F \propto \sqrt{E_F}$ and $P_z \propto 1/\sqrt{E_F}$ [23]. For a typical semiconductor such as InGaAs/InAlAs heterostructure [36], the effective mass $m^* = 0.05m_e$, with m_e the free electron mass, and the Rashba spin-orbit coupling $\alpha_R \approx 10$ meV $\cdot$ nm. One estimates [23] that the peak value of $P_z \approx 2.4\%$ if $E_F \approx 3.3$ meV, and $P_z \approx 0.4\%$ for a more realistic value of $E_F \approx 100$ meV corresponding to the 2D electron density $n_{2D} \approx 2.1 \times 10^{12}$ cm^{-2}. Therefore, the local spin polarization we predicted on the TI surface is about 50 times larger than that in a typical 2D semiconductor. In some metallic Rashba surfaces, the spin-orbit coupling is larger. However, the MSHE is still much smaller than that in TI. Taking Au(111) as an example, $\alpha_R \approx 33$ meV $\cdot$ nm, and $E_F \approx 475$ meV [37]. We have $P_z \approx 1.5\%$, about 10 times smaller than that on the surface of the TI. We also note that the predicted MSHE in a HgTe quantum well by applying an in-plane potential gradient is about 1000 times smaller than that in the TI [26,38].

We now briefly discuss the effect of the shape of the potential to the spin polarization. It has been shown [28] that the total spin polarization across the junction is a constant, independent of the potential shape. Therefore, if the shape of the potential varies, the spatial profile of the spin polarization is expected to vary, but the sum of the spin polarization remains the same and relatively large on the surface of the TI. The oscillation period shown in Fig. 3 is approximately inversely proportional to the Fermi wave vector. We expect a deviation of the potential shape in length scale which is smaller than the oscillation period would not affect the results significantly.

In summary, we have theoretically examined the mesoscopic spin Hall effect on the surface of three-dimensional topological insulator with a step-function potential. In the ballistic transport regime, a giant spin polarization oscillation across the junction is induced by a transverse electric current. The spin polarization is estimated to be as large as 20%, which is insensitive to the Fermi level and not confined by the potential step. Its magnitude is about one or two orders larger than that in 2D electron gas with Rashba spin-orbit coupling. The spatial oscillation period is of order of the inverse of the Fermi wave vector. These features are markedly distinguished from the 2D electron gas and observable in spin resolved scanning tunneling microscope.

We acknowledge financial support from HKSAR RGC Grants No. HKU 701010 and No. CRF HKU 707010. Y. Z. is supported by the National Basic Research Program of China (973 Program, No. 2011CBA00103), NSFC (No. 11074218), and PCSIRT (No. IRT0754).

[1] C. L. Kane and E. J. Mele, Phys. Rev. Lett. **95**, 146802 (2005); L. Fu, C. L. Kane, and E. J. Mele, Phys. Rev. Lett. **98**, 106803 (2007).
[2] B. A. Bernevig *et al.*, Science **314**, 1757 (2006); M. Konig *et al.*, Science **318**, 766 (2007).
[3] X.-L. Qi and S.-C. Zhang, Phys. Today **63**, 33 (2010); arXiv:1008.2026.
[4] M. Z. Hasan and C. L. Kane, arXiv:1002.3895.
[5] J. E. Moore and L. Balents, Phys. Rev. B **75**, 121306 (2007).
[6] D. Hsieh *et al.*, Nature (London) **452**, 970 (2008).
[7] Y. Xia *et al.*, Nature Phys. **5**, 398 (2009).
[8] T. Zhang *et al.*, Phys. Rev. Lett. **103**, 266803 (2009).
[9] H. J. Zhang *et al.*, Nature Phys. **5**, 438 (2009).
[10] Y. K. Kato *et al.*, Science **306**, 1910 (2004).
[11] V. Sih *et al.*, Nature Phys. **1**, 31 (2005).
[12] J. Wunderlich *et al.*, Phys. Rev. Lett. **94**, 047204 (2005).
[13] S. O. Valenzuela and M. Tinkham, Nature (London) **442**, 176 (2006).
[14] J. E. Hirsch, Phys. Rev. Lett. **83**, 1834 (1999).
[15] Shufeng Zhang, Phys. Rev. Lett. **85**, 393 (2000).
[16] H. A. Engel, B. I. Halperin, and E. I. Rashba, Phys. Rev. Lett. **95**, 166605 (2005).
[17] W.-K. Tse and S. DasSarma, Phys. Rev. Lett. **96**, 056601 (2006).
[18] S. Murakami, N. Nagaosa, and S.-C. Zhang, Science **301**, 1348 (2003); Phys. Rev. B **69**, 235206 (2004).
[19] J. Sinova *et al.*, Phys. Rev. Lett. **92**, 126603 (2004).
[20] S. Murakami, Adv. Solid State Phys. **45**, 197 (2005).
[21] H. A. Engel, *et al.*, *Handbook of Magnetism and Advanced Magnetic Materials* (Wiley, Chichester, 2007).
[22] B. K. Nikolic *et al.*, Phys. Rev. Lett. **95**, 046601 (2005).
[23] V. A. Zyuzin, P. G. Silvestrov, and E. G. Mishchenko, Phys. Rev. Lett. **99**, 106601 (2007); P. G. Silvestrov, V. A. Zyuzin, and E. G. Mishchenko, Phys. Rev. Lett. **102**, 196802 (2009).
[24] G. Usaj and C. A. Balseiro, Europhys. Lett. **72**, 631 (2005);
[25] J. Yao and Z. Q. Yang, Phys. Rev. B **73**, 033314 (2006).
[26] Y. Xing *et al.*, Phys. Rev. B **74**, 155313 (2006).
[27] P. Bokes, F. Corsetti, and R. W. Godby, Phys. Rev. Lett. **101**, 046402 (2008); P. Bokes and F. Horvath, Phys. Rev. B**81**, 125302 (2010).
[28] P. G. Silvestrov and E. G. Mishchenko, arXiv:0912.4658.
[29] H.-Z. Lu *et al.*, Phys. Rev. B **81**, 115407 (2010).
[30] J. Chen *et al.*, Phys. Rev. Lett. **105**, 176602 (2010).
[31] Yi Zhang *et al.*, Nature Phys. **6**, 584 (2010).
[32] W. L. McMillan, Phys. Rev. **175**, 559 (1968); S. Kashiwaya and Y. Tanaka, Rep. Prog. Phys. **63**, 1641 (2000).
[33] See supplementary material at http://link.aps.org/supplemental/10.1103/PhysRevLett.106.057205 for the expressions given in detail.
[34] M. I. Katsnelson *et al.*, Nature Phys. **2**, 620 (2006).
[35] S. Datta, *Electronic Transport in Mesoscopic Systems* (Cambridge University Press, Cambridge, England, 1995).
[36] J. Nitta *et al.*, Phys. Rev. Lett. **78**, 1335 (1997).
[37] D. Malterre, *et al.*, New J. Phys. **9**, 391 (2007);
[38] Y. S. Gui *et al.*, Phys. Rev. B **70**, 115328 (2004).